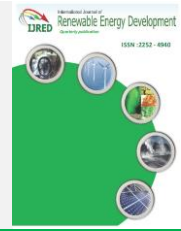




Contents list available at IJRED website

Int. Journal of Renewable Energy Development (IJRED)

Journal homepage: <https://ijred.undip.ac.id>



Research Article

Numerical Modeling of $\text{CuIn}_x\text{Ga}_{(1-x)}\text{Se}_2/\text{WS}_2$ Thin Solar Cell with an Enhanced PCE

Youcef Belhadji*

Department of Electrical Engineering, University of Tiaret, 14000, Algeria

Abstract. Designing thin film solar cells with high and stable output performance under different operating points remains a large area of research. In the context of Chalcopyrite-based solar cells ($\text{CuIn}_x\text{Ga}_{(1-x)}\text{Se}_2$) where the buffer layer is CdS, great progress has been made but research is still underway to optimize their performance. Besides the environmental concerns and limiting factors of CdS material, the use or combination of new materials like ZnS, ZnSe and WS_2 as a buffer layer is solicited. Due to these attracted optical and crystallographic properties, Tungsten Disulfide: WS_2 is solicited during the last years. Through numerical simulation, we investigate in this work the dc parameters of $\text{CuIn}_x\text{Ga}_{(1-x)}\text{Se}_2/\text{WS}_2$ solar cell with reduced buffer layer thickness of 30 nm. Considering the presence of neutral and divalent defects in the absorber layer, simulations are performed under the impact of temperature, concentration of charge carriers in WS_2 layer and light spectrum change. The divalent defects taken into account are: double donors / acceptors and amphoteric having a Gaussian distribution. For more calculation precision and in order to obtain the desired performance of the solar cell, the impact of series and shunt resistors is also considered. In comparison with results reported in previous works, carried out on the $\text{CuIn}_x\text{Ga}_{(1-x)}\text{Se}_2/\text{WS}_2$ solar cell, a remarkable improvement in the performance of the solar cell is achieved. When temperature increase by 10K, the short circuit current and open circuit voltage are enhanced by $\sim 0,05\text{mA}/\text{cm}^2$ and $\sim 0,0022$ respectively. The optimal values of the solar cell parameters obtained in this study are: $J_{sc} \approx 31,0683$ (mA/cm^2), $V_{oc} = 1,0173$ (V), $\text{PCE} = 26,72\%$ and $\text{FF} = 84,54\%$.

Keywords: WS_2 , $\text{CuIn}_x\text{Ga}_{(1-x)}\text{Se}_2$, divalent defect, thin film, scaps-1d

Article History: Received: 23rd May 2021; Revised: 21st July 2021; Accepted: 24th Dec 2021; Available online: 14th January 2022

How to Cite This Article: Belhadji, Y. (2022) Numerical Modeling of $\text{CuIn}_x\text{Ga}_{(1-x)}\text{Se}_2/\text{WS}_2$ Thin Solar Cell with an Enhanced PCE. *International Journal of Renewable Energy Development*, 11(2), 393-401
<https://doi.org/10.14710/ijred.2022.38527>

1. Introduction

The use of thin films with excellent structural, physicochemical and optical properties has a significant impact in improving the performance of solar cells. The distinctive properties of Cadmium telluride (CdTe), Kesterite ($\text{Cu}_2\text{ZnSnSe}_4$), perovskite halide ($\text{CH}_3\text{NH}_3\text{PbI}_3$) and Chalcopyrite ($\text{CuIn}_x\text{Ga}_{(1-x)}\text{Se}_2$, CIS, CGS), allowed them to take a promising place in solar cells manufacturing with high power conversion efficiency (PCE). Among the materials mentioned above, the quaternary composite $\text{CuIn}_x\text{Ga}_{(1-x)}\text{Se}_2$ is qualified as a good absorber for second generation solar cells. The encouraging properties of $\text{CuIn}_x\text{Ga}_{(1-x)}\text{Se}_2$ are: direct gap, low manufacturing cost and high absorption coefficient. Another interesting property is the controlled energy gap which directly depends on the composition of gallium atoms. Without changing their photovoltaic properties, the $\text{CuIn}_x\text{Ga}_{(1-x)}\text{Se}_2$ has the ability to accommodate large deviations from the stoichiometry coefficient (Igalson *et al.*, 2005). The main structure of $\text{CuIn}_x\text{Ga}_{(1-x)}\text{Se}_2$ based solar cell is formed by a set of thin layers deposited on a flexible (rigid) support as following: front contact/ windows layer/buffer layer/absorber layer/Back contact.

- The front contact (or electrode) is formed on thin conductive oxide (TCO).
- The window layer is generally formed by intrinsic or Al-doped ZnO.
- The p-doped $\text{CuIn}_x\text{Ga}_{(1-x)}\text{Se}_2$ is stacked as an absorber layer. His controlled band gap allow absorbing a wide range of the sunlight spectrum (Belhadji, 2020), (Frisk *et al.*, 2014), (Aissani *et al.*, 2017).
- The thin n-CdS buffer layer is placed for the purpose of adjusting the width of the band gap between the absorber and the window layer and improving the performance of the solar cell.
- Because of its excellent conductivity, molybdenum (Mo) is well suited as a back contact. Also, it does not react strongly with $\text{CuIn}_x\text{Ga}_{(1-x)}\text{Se}_2$ (Ong *et al.*, 2018). For good collection of photo-generated charge carriers, Mo is often deposited as coated soda-lime glass (SLG) (Kumar and Singh, 2020) or flexible Mo foils (Gremenok *et al.*, 2015), (Dhere *et al.*, 2002).

However, significant progress in improving the performance of $\text{CuIn}_x\text{Ga}_{(1-x)}\text{Se}_2$ solar cells is being made and research in this context is still ongoing. In the majority of studies performed, the usual buffer layer is generally a thin n-CdS. A PCE record lab of 23.35% has

* Corresponding author: youcef.belhadji@univ-tiaret.dz

been achieved for Cd-Free $\text{Cu}(\text{In},\text{Ga})(\text{Se},\text{S})_2$ thin-film solar cell (Nakamura et al., 2019). Despite PCE has been significantly boosted using CdS, the toxicity of Cadmium remains a major limiting factor. As a solution, research is directed towards the use of other materials with good photoelectric characteristics. Known as a transition-metal Dichalcogenides (TMDC) like $\text{MoS}(\text{Se},\text{S})_2$ and $\text{WS}(\text{Se},\text{S})_2$, the Tungsten Disulfide (WS_2) is recently investigated as an excellent buffer layer for thin film solar cells. The electronic and optical properties of ultra-thin 2D- WS_2 , were studied by Sayan Roy and Peter Bermel (Roy and Bermel, 2018). Many other works on WS_2 based solar cell are published where an efficiency enhancement is observed. The thin film WS_2 was successfully incorporated for the first time as a window layer in CdTe/WS_2 solar cell by Bin Rafiq and their collaborators (Bin Rafiq et al., 2020). Yuanbao Lin et al. also studied an organic solar cell with WS_2 as HTL that exhibit a highest PCE of 17% (Lin et al., 2019). Further work by Sobab et al. (2020) where WS_2 was incorporated as an absorbent layer with back reflector. The maximum efficiency recorded for this cell is equal to 20% (Sobab et al., 2020). Afterwards, a multitude solar cell structure using WS_2 layer are investigated (either as an absorbent or buffer layer) (Shanmugam et al. 2012), (Debbarma, et al. 2018), (Bin Rafiq et al., 2020), (Sobayela et al., 2020), (Kumar and Singh, 2020), (Patel and Pandey, 2020) and (Rashidi et al., 2020). These works didn't fail to indicate that WS_2 is a potential material for the photovoltaic applications. In the case of $\text{CuIn}_x\text{Ga}_{(1-x)}\text{Se}_2$ solar cell, a poor works are founded in literature. The first and new CIGS/ WS_2 solar cell was proposed and numerically modeled by Sobayel et al. (Sobayelb et al., 2020). The studied structure provides power conversion efficiency (PCE) of 26.4%. Based on this work, we proposed to optimize the physical and geometrical parameters of the solar cell using the SCAPS-1D simulator. The obtained results will be discussed and compared with those registered for the $\text{CuIn}_x\text{Ga}_{(1-x)}\text{Se}_2/\text{CdS}$ and previous work carried out on the $\text{CuIn}_x\text{Ga}_{(1-x)}\text{Se}_2/\text{WS}_2$ solar cell.

2. Solar cell design and calculation methodology

2.1 Solar cell design

Using a predefined SCAPS-1D model and the work of Sobayel et al. (Sobayela et al., 2020), the solar cell was designed by stacking five layers as shown in Figure 1. The choice and optimization of the layer thicknesses are primordial to obtain the desired improvement. In this work, a thin buffer layer WS_2 , with $0.03 \mu\text{m}$ thick, is inserted into the heterojunction formed between the $\text{CuIn}_x\text{Ga}_{(1-x)}\text{Se}_2$ and ZnO layers. The ZnO layer has a thickness of $0.230 \mu\text{m}$ with a concentration set at 1.10^5 cm^{-3} . As mentioned in many studies, the maximum absorption and optimal performance are achieved with a $\text{CuIn}_x\text{Ga}_{(1-x)}\text{Se}_2$ absorber thickness ranging from 1 to $3 \mu\text{m}$ (AlZoubi and Moustafa, 2019), (Belhadji, 2020), (Rai and Dwivedi, 2020), (Daoudia et al., 2016). The PCE record is obtained with 2-3 μm thick films (Goffard et al., 2017). For a thickness of about $1 \mu\text{m}$ the PCE remained optimal (Pettersson et al., 2013), (Lundberg et al., 2003), (Sharaman et al., 1997). In the present study we adopted a $\text{CuIn}_x\text{Ga}_{(1-x)}\text{Se}_2$ with a thickness of $2.5 \mu\text{m}$ and a band gap of 1.68 eV in order to maximize the absorption. In addition, the performance of CIGS thin film solar cells is significantly affected by the presence of deep level and native defects (Kerr et al., 2004). For that, three types of defects are considered: Neutral double Acceptor/Donor and Amphoteric. Their distribution is chosen Gaussian. Other optical properties such as capture and emission sections, density as well as defect energy level are also defined. For WS_2 buffer layer, two defects are included: neutral and single donor with uniform distribution. The properties of the front and back contacts such as metal work function as well as majority carrier barrier height are adjusted. The main input parameters used in the simulation are filled in Tables 1, 2 and 3.

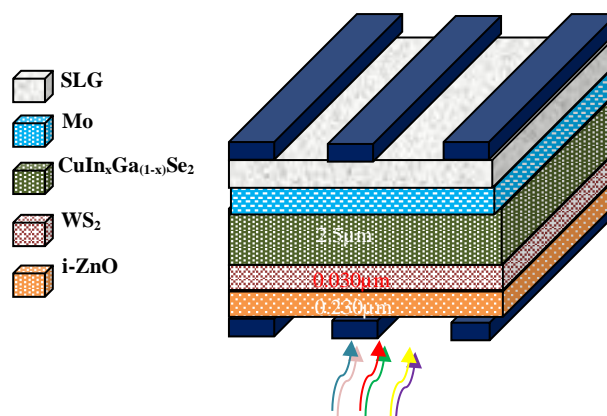


Fig. 1 The $\text{CuIn}_x\text{Ga}_{(1-x)}\text{Se}_2/\text{WS}_2$ solar cell structure

Table 1
The physical parameters of each layer

Parameters	Layers			
	P-CuIn _x Ga _(1-x) Se ₂	n-WS ₂	n-CdS	i-ZnO
Thickness (μm)	2.5	0.030	0.030	0.230
Bandgap (eV)	1.68	1.68	2.4	3.4
χ(eV)	3.90	3.90	4.2	4.5
ε _r	13.60	13.60	10.00	9.0
N _C (cm ⁻³)	2.2 × 10 ¹⁸	2.2 × 10 ¹⁸	2.2 × 10 ¹⁸	3.0 × 10 ¹⁸
N _V (cm ⁻³)	1.8 × 10 ¹⁹	1.8 × 10 ¹⁹	1.8 × 10 ¹⁹	1.7 × 10 ¹⁹
Electron thermal velocity (cm/s)	1.0 × 10 ⁷	1.0 × 10 ⁷	1.0 × 10 ⁷	1.0 × 10 ⁷
Hole thermal velocity (cm/s)	1.0 × 10 ⁷	1.0 × 10 ⁷	1.0 × 10 ⁷	1.0 × 10 ⁷
μ _n (cm ² /Vs)	100	100	100	100
μ _p (cm ² /Vs)	25	25	25	25
N _D (cm ⁻³)	10	8.0 × 10 ¹⁸	8.0 × 10 ¹⁸	1.0 × 10 ⁵
N _A (cm ⁻³)	5.0 × 10 ¹⁷	1.0	1.0	1.0 × 10 ⁵

Table 2
The main parameters of the front and back contacts

Contacts	Parameters	
	Front contact	Back contact
Metal work function (eV)	4.45	5.4
Electron surface recombination velocity (cm/s)	1.00 × 10 ⁷	1.00 × 10 ⁷
Hole surface recombination velocity (cm/s)	1.00 × 10 ⁷	1.00 × 10 ⁷
Majority carrier barrier height (eV)	Electron: 3.45	Electron: 0.78

Table 3
The defect properties

Defect types	CuIn _x Ga _(1-x) Se ₂		
	Double acceptor	Double donor	Amphoteric
Distribution	Gaussian	Gaussian	Gaussian
Characteristic energy (eV) (above Ev)	0.24	0.3	0.6
Trap concentration N _t (cm ⁻³)	1.0 × 10 ¹⁵	1.0 × 10 ¹⁵	1.0 × 10 ¹⁵
Capture cross- section	σ _p = 1.0 × 10 ⁻¹⁹ σ _n = 1.0 × 10 ⁻¹⁹	σ _p = 1.0 × 10 ⁻¹⁹ σ _n = 1.0 × 10 ⁻¹⁹	σ _p = 1.0 × 10 ⁻¹⁹ σ _n = 1.0 × 10 ⁻¹⁹
Defect types	n-WS ₂ (n-CdS)		
	Neutral	Single Donor	----
Distribution	Uniform	Uniform	----
Characteristic energy (eV) (above Ev)	0.1	0.3	----
Trap concentration N _t (cm ⁻³)	2.0 × 10 ¹⁵	1.1 × 10 ¹⁴	----
Capture cross- section	σ _p = σ _n = 1.0 × 10 ⁻¹	σ _p = σ _n = 1.0 × 10 ⁻¹	---
Defect types	i-ZnO		
	Neutral	----	----
Distribution	Single	----	----
Characteristic energy (eV) (above Ev)	1.650	---	---
Trap concentration N _t (cm ⁻³)	1.0 × 10 ¹⁵	----	----

2.2 Calculation Methodology

SCAPS-1D simulator enables numerical simulation of dc and ac behavior of multilayer thin film solar cells. Based on the physical parameters of each layer, the simulator has the ability to solve the continuity and Poisson equations governing the transport of charges in semiconductors. The layers parameters can be easily filled and modified as input data. It also offers the possibility of

simulating defects with a fixed number of possible states of charge equal to five. We note N_s the defect density in a specified state 's' and the recombination rate U^{s+1/2}. This rate is related to the transitions from state 's' to state 's+1'. The net electron and hole capture rates are represented by

$$U_n^{s+\frac{1}{2}}, U_p^{s+\frac{1}{2}} \text{ where are expressed as follows:}$$

$$\begin{cases} U_n^{s+\frac{1}{2}} = nC_n^{s+\frac{1}{2}}N_s - e_n^{s+\frac{1}{2}}N_{s+1} \\ U_p^{s+\frac{1}{2}} = pC_p^{s+\frac{1}{2}}N_{s+1} - e_p^{s+\frac{1}{2}}N_{s+1} \end{cases} \quad (1)$$

e_n, e_p, c_n and c_p represent the emission and capture coefficients of the electrons and holes respectively.

The theory of detailed balance is applied to determine the emission coefficient. Their expressions are given as follows:

$$\begin{cases} e_n^{s+\frac{1}{2}} = N_C C_n^{s+\frac{1}{2}} \frac{g_s}{g_{s+1}} \exp\left(-\frac{E_C - E_t^{s+\frac{1}{2}}}{kT}\right) \\ e_p^{s+\frac{1}{2}} = N_V C_p^{s+\frac{1}{2}} \frac{g_{s+1}}{g_s} \exp\left(-\frac{E_t^{s+\frac{1}{2}} - E_V}{kT}\right) \end{cases} \quad (2)$$

Where N_C and N_V are the effective density of state in the conduction and valence band respectively. “g” is the degeneracy of charge state and E_t define the energy level of the defect.

However, for more accurate modelling of the solar cell behaviour, a simple diode equivalent model is used (Figure 2). The model takes in account the impact of series and shunt resistances. In this case, the current density “J” of the solar cell can be expressed as follow:

$$J_{(\text{solar-cell})} = J_L - J_D - J_{sh} \quad (3)$$

Where J_L represent the light induced current density, J_D is the current density associated to the diode which models the recombination losses where those due to the shunt resistance are modeled by J_{sh} . The resistance R_s models the solar cell internal losses (Ghani *et al.*, 2013):

- Front and back contacts resistances,
- Lead resistance,
- Ohmic contact.

Taking all these factors into account, we can write:

$$J_{\text{solar cell}} = J_L - J_0 \left[\exp\left(\frac{V + R_s J_{\text{solar cell}}}{nV_{th}}\right) - 1 \right] - \frac{V + R_s J_{\text{solar cell}}}{R_{sh}} \quad (4)$$

With $V_{th} = \frac{kT}{q}$ represents the thermal voltage

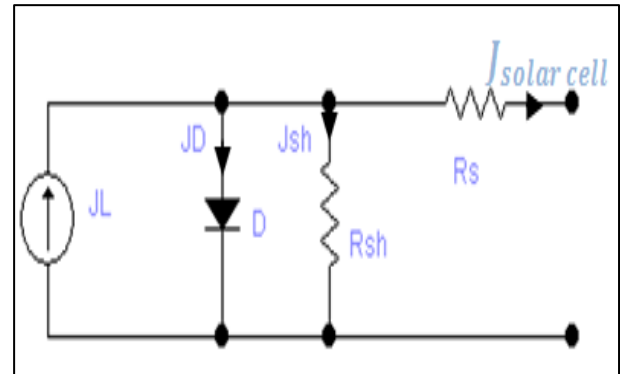


Fig. 2 the equivalent single-diode model of the solar cell

3. Results and Discussion

3.1 J-V and QE curves

The number of photo-generated charge carriers in an illuminated solar cell is called quantum efficiency denoted QE. It translates a measure of the fraction of incident photons converted into electric current. By integrating the product of the external QE and the density of photon flux, the total current density can be easily calculated. The QE and J-V curves of the simulated solar cell are depicted in Figures 3, 4 and 5. These curves are obtained at room temperature without considering the presence of series (R_s) and shunt (R_{sh}) resistances. From Figures 2 and 3, the obtained QE using WS₂ is close to that obtained with CdS layer except a small decrease observed for wavelengths ranging from 400 to 500 nm. The dc output performances deduced from the J-V curves are given in Table 4. In comparison with the results obtained for the CuIn_xGa(1-x)Se₂/CdS solar cell, the parameters Voc, Jsc, FF and PCE are too close. Consequently, WS₂ can be considered as a good solution to replace CdS layer as well to overcome the problem of its toxicity. On another side, a new remarkable enhancement of PCE and short current has been recorded. Therefore, a Jsc about 31.063 mA/cm² is obtained against a value of 29.57 mA/cm² registered by K. Sobayel *et al.* (Sobayela *et al.*, 2020). The improvement of the short-circuit current density is more attached to the low band gap and the optimized thickness of the WS₂ layer. This latter promotes more collecting of electron/hole pairs photo-generated in the layer. It also provokes compensation for reduced optical reflections induced in the case of thicker buffer layer.

Table 4
 Comparison of dc parameters of the CuIn_xGa(1-x)Se₂/WS₂ and CuIn_xGa(1-x)Se₂/CdS solar cells

DC Parameters	Voc (V)	Jsc (mA/cm ²)	FF (%)	PCE (%)
n_WS ₂	1.0172	31.062942	84.51	26.70
n_CdS	1.0173	31.258042	84.54	26.88
(Sobayela <i>et al.</i> 2020)	1.026	29.57	86.96	26.40

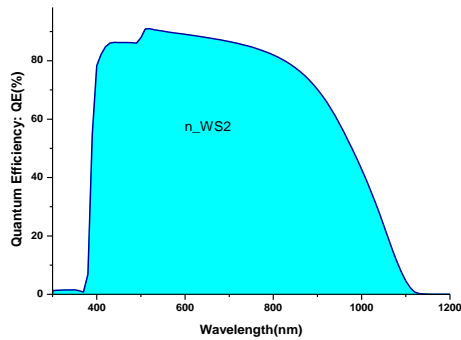


Fig. 3 Quantum efficiency of $\text{CuIn}_x\text{Ga}_{(1-x)}\text{Se}_2/\text{WS}_2$ solar cell

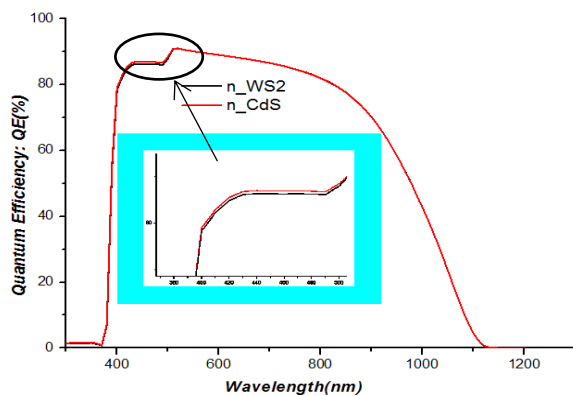


Fig. 4 Comparison of the quantum efficiency of $\text{CuIn}_x\text{Ga}_{(1-x)}\text{Se}_2/\text{WS}_2$ and $\text{CuIn}_x\text{Ga}_{(1-x)}\text{Se}_2/\text{CdS}$ solar cells

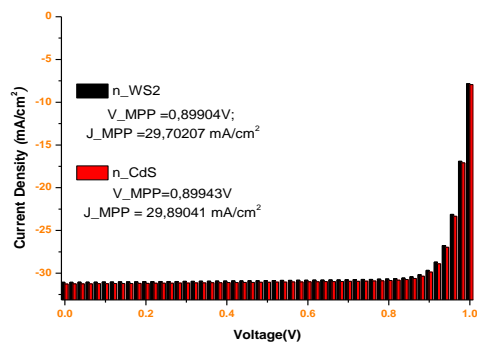


Fig. 5 Comparison of the J-V curves of the $\text{CuIn}_x\text{Ga}_{(1-x)}\text{Se}_2/\text{WS}_2$ and $\text{CuIn}_x\text{Ga}_{(1-x)}\text{Se}_2/\text{CdS}$ solar cells

3.2 DC parameters as function of temperature

When designing and manufacturing solar cells, the study of the effect of temperature remains crucial and need to be taken into consideration. Thereby, investigating the temperature effect on the performance of solar cells has a great relevance. Especially for space applications where panels are exposed to temperatures ranging from 80 to 380K within a few minutes after eclipse (Liu, *et al.*, 2005). However, the impact of temperature on the dc parameters

of the $\text{CuIn}_x\text{Ga}_{(1-x)}\text{Se}_2$ solar cell was drawn more attention. It's numerically and experimentally studied by many authors (Eisenbarth *et al.*, 2010), (Fathi *et al.*, 2015), (Zaidi *et al.*, 2019), (N.M. Ravindra & L. Lin, 2020) and (Sobayela *et al.*, 2020) where all of these authors have underlined its significant influence. In this section, we present the results of investigation of the losses (or enhancement) brought about the temperature change from 263.15 to 243.15K with a step of 10K. From the results filled in table 5, the impact of temperature is clearly visible. When temperature increase by 10K the short circuit current and open circuit voltage are enhanced by $\sim 0.05\text{mA}/\text{cm}^2$ and ~ 0.0022 respectively. According to the relation of energy gap temperature dependence commonly known Varshni relation, the temperature increases induce band gap energy (E_g) decreases. Hence, it contributes to an enhancement of the short current density (J_{sc}). For the fill factor, a slight decrease is observed when temperature increase. The solar cell efficiency (PCE) is slightly increases until $T^\circ=293.15\text{K}$ to reach his optimal value of 26.70%. For more temperature increase, the probabilities of charges recombination and thermal agitation also increase. Then, it will lead to a reduction of PCE (Fan JCC, 1986). The impact of temperature on the V_{MPP} voltage and J_{MPP} current (equivalent to the maximum power point) is also investigated. The PCE, is slightly increases until $T^\circ=293.15\text{K}$ and reached his optimal value of 26.70%. The impact of temperature on the voltage V_{MPP} and J_{MPP} current, equivalent to the maximum power point, is also investigated. The registered results are plotted in Figure 6. From the curve, the current J_{MPP} increased and reach its maximum value of 29.77% when temperature increases from 263.15K to 343.15K. For the voltage V_{MPP} , a maximum value equal to 0.9V is achieved for a temperature $T=273.15\text{K}$.

From Figure 7, we clearly observe that the gradient of temperature on the quantum efficiency was restricted. For long wavelengths (photons with low energy), a small increase was observed with temperature increases.

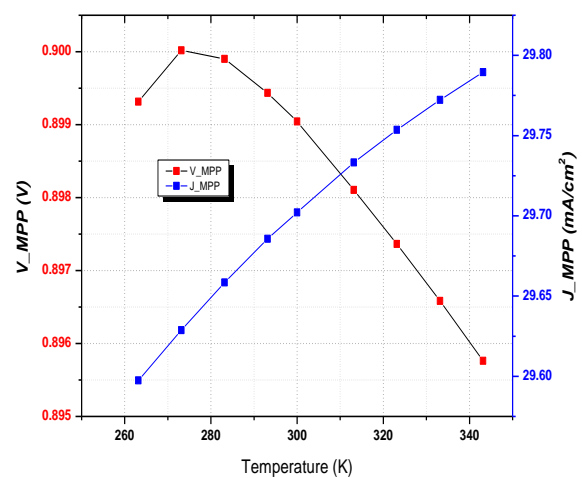


Fig. 6 Dependence of V_{MPP} and J_{MPP} on the temperature

Table 5
 Voc, Jsc, FF and PCE of the solar cell as function of temperature change

DC Parameters /T°	Voc (V)	Jsc(mA/cm ²)	FF(%)	PCE(%)
263.15	30.885865	1.0091	85.40	26.62
273.15	30.937767	1.0113	85.23	26.67
283.15	30.986581	1.0135	84.99	26.69
293.15	31.032700	1.0157	84.71	26.70
300.00	31.062942	1.0172	84.51	26.70
313.15	31.118521	1.0200	84.13	26.70
323.15	31.159236	1.0221	83.84	26.70
333.15	31.199320	1.0240	83.55	26.69
343.15	31.239491	1.0260	83.26	26.68

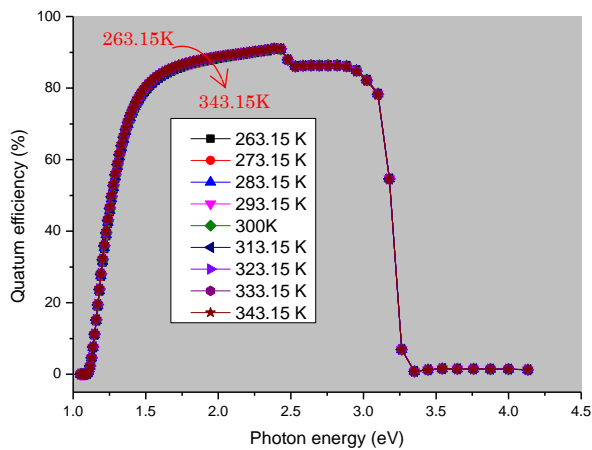


Fig. 7 Quantum efficiency as function of temperature

3.3 Impact of shunt and series resistances

To analyze the impact of series and shunt resistances we fixed the shunt resistance: R_{sh} equal to $1.104 \Omega \cdot \text{cm}^2$. The series resistance is varied from 0.1 to $1 \Omega \cdot \text{cm}^2$. According to the curves shown in Figure 8, the Voc voltage was not affected by the R_s change while a slight decrease was recorded for Jsc and PCE. The impact of the resistance R_s was remarkable on the fill factor. It results in a reduction of 84% to 81.54% when R_s varies from $0.1 \Omega \cdot \text{cm}^2$ to $1.0 \Omega \cdot \text{cm}^2$ respectively. Moreover, the increase of R_s causes a rapid decrease of the maximum power point MPP (Figure 9).

3.4 Impact of incident light spectrum

The purpose of the solar cell is to convert the light spectrum into electricity. The change in intensity of the incident light spectrum or illumination has a direct impact on their performance. In Figure 10, the evolution of the J-V curves is studied for three spectra of incident light: 400 nm, AM1.5G and AM1.5D. From these curves, the current densities obtained for AM1.5G and AM1.5D spectrum are too close while a remarkable degradation is recorded for 400nm spectrum. The maximum absorption given the highest PCE are recorded for the AM1.5G spectrum.

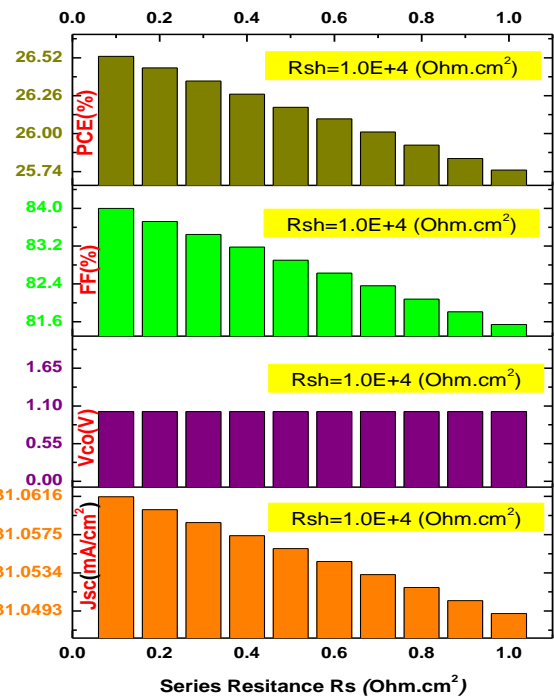


Fig. 8 Dependence of dc parameters of the solar cell as function of series resistance change (R_{sh} equal to $1.0E+4 \Omega \cdot \text{cm}^2$)

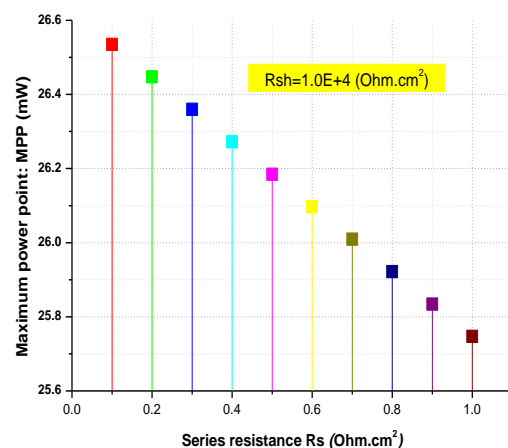


Fig. 9 Evolution of the MPP of the $\text{CuIn}_x\text{Ga}_{(1-x)}\text{Se}_2/\text{WS}_2$ solar cell as function of series resistance (R_{sh} equal to $1.0E+4 \Omega \cdot \text{cm}^2$)

3.5 Impact of high carrier concentration of WS₂ buffer layer

We report in this section the results of investigation of high carrier concentration, of the WS₂ buffer layer, on the dc parameters. The carrier concentration is varied from $8.10^{18} \text{ cm}^{-3}$ to $1.10^{20} \text{ cm}^{-3}$. The results of V_{co} , J_{sc} , FF and PCE are shown in Figure 11. From the curves, the impact of carrier concentration was significant on solar cell parameters. They increase with increasing concentration and become optimal for higher doping concentrations. As the concentration increases, it will lead to a reduction of the potential barrier in the WS₂/CuIn_xGa_(1-x)Se₂ and ZnO/CdS interfaces. It subsequently causes a widening of the space charge zone (ZCE). Therefore, the result is an improvement in the collection of the photo-generated electron-hole pairs and hence an improvement in all parameters of the solar cell (Dabbabi *et al.*, 2017).

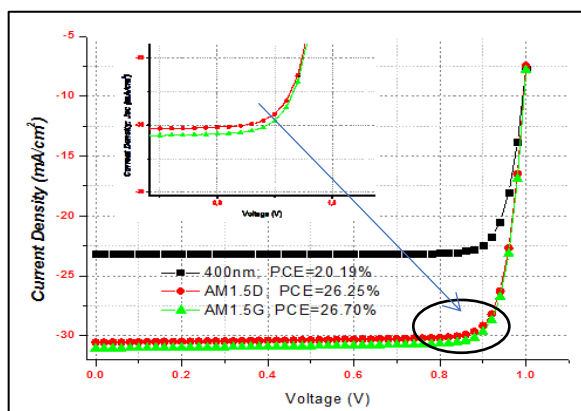


Fig. 10 J-V curves of the CuIn_xGa_(1-x)Se₂/WS₂ solar cell for three light spectrum: 400nm, AM1.5G and AM1.5D

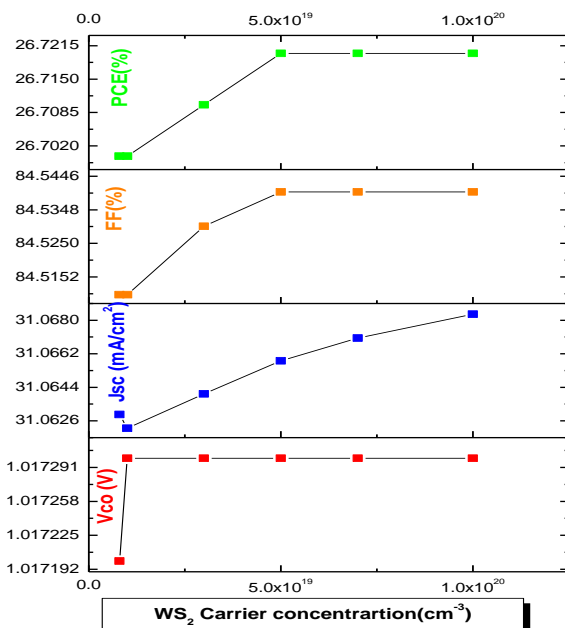


Fig. 11 PCE, FF, J_{sc} and V_{oc} as function of WS₂ carriers' concentration

6. Conclusion

A numerical modeling of the CuIn_xGa_(1-x)Se₂-based solar cell, with a 30 nm thick WS₂ buffer layer was presented in this paper. The performances of the solar cell were extracted using the SCAPS-1D simulator and under the effect of the variation of the temperature, the concentration of charge carriers, the light spectrum as well as the effect of the series and shunt resistances. The simulations are also carried out considering the presence of defects in the three layers: CuIn_xGa_(1-x)Se₂, WS₂ and ZnO. According to the obtained results, the considered defects did not constitute recombination centers strongly degrading the performance of the solar cell. Additionally, using WS₂ as a buffer layer improved the output performance. We found that PCE exhibited slight temperature dependence where it dropped from 26.62% to 26.70% as the temperature increased from 263.15 K to 323.15 K. For more temperature rise, a small degradation was observed. Regarding the concentration of charge carriers in the buffer layer, its increase induces an increase in all parameters: V_{co} , J_{sc} , FF as well as PCE. In comparison with previous work on the CuIn_xGa_(1-x)Se₂/WS₂ solar cell, a new optimal and stable PCE of 26.72% was recorded for a concentration of up to $5.10^{19} \text{ cm}^{-3}$. On the other hand, the quantum efficiency obtained was very close to that obtained by CdS. This result proves the importance of the material WS₂ to overcome the problem of toxicity of CdS. Furthermore, three light spectra are studied: 400 nm, AM1.5G and AM1.5D where the highest PCE is obtained for the AM1.5G spectrum. For possible improvements, this work can constitute a useful information support for the understanding and the design of solar cells based on CuIn_xGa_(1-x)Se₂/WS₂ with a stable performance in the face of temperature variations and light spectrum temperature change. So design a solar cell more suited to terrestrial and space applications.

References

- Aissani, H., Helmaoui, A., Moughli, H. (2017) Numerical Modeling of Graded Band-Gap CIGS Solar Cell for High Efficiency, International Journal of Applied Engineering Research, 12(02), 227-232
- AlZoubi, T., & Moustafa, M. (2019) Numerical optimization of absorber and CdS buffer layers in CIGS solar cells using SCAPS. SGCE 291–298; <https://doi.org/10.12720/sgce.8.3.291-298>
- Belhadji, Y., (2020) The band gap and Ga-composition grading profiles effect on the performance of 1μm thin film graded-CIGS solar cell, in: 2020 6th IEEE International Energy Conference (ENERGYCon). 360–365; <https://doi.org/10.1109/ENERGYCon48941.2020.9236491>
- Bin Rafiq, Md.K.S., Amin, N., Alharbi, H.F., Luqman, M., Ayob, A., Alharthi, Y.S., Alharthi, N.H., Bais, B., Akhtaruzzaman, Md. (2020) WS₂: A New Window Layer Material for Solar Cell Application. Sci Rep 10, 771; <https://doi.org/10.1038/s41598-020-57596-5>
- Dabbabi, S., Ben Nasr, T., Kamoun-Turki, N. (2017) Parameters optimization of CIGS solar cell using 2D physical modeling. Results in Physics 7, 4020–4024; <https://doi.org/10.1016/j.rinp.2017.06.057>
- Daoudia, A.K., El Hassouani, Y., Benami, A. (2016) Investigation of the effect of thickness, band gap and temperature on the efficiency of CIGS solar cells through SCAPS-1D 6(2), 71-75.

- Debbarma, R., Behura, S. K., Wen, Y., Che, S. and Berry, V. (2018) WS_2 -induced enhanced optical absorption and efficiency in graphene/silicon heterojunction photovoltaic cells. *Nanoscale*, 10, 20218–20225. <https://doi.org/10.1039/c8nr03194k>
- Dhere, N.G., Ghongadi, S.R., Pandit, M.B., Jahagirdar, A.H., Scheiman, D. (2002) CIGS2 thin-film solar cells on flexible foils for space power. *Prog. Photovolt: Res. Appl.*, 10, 407–416; <https://doi.org/10.1002/pip.447>
- Eisenbarth, T., Unold, T., Caballero, R., Kaufmann, C.A., Schock, H.-W. (2010) Interpretation of admittance, capacitance-voltage, and current-voltage signatures in $\text{Cu}(\text{In,Ga})\text{Se}_2$ thin film solar cells. *Journal of Applied Physics*, 107, 034509; <https://doi.org/10.1063/1.3277043>
- Fan JCC (1986) Theoretical temperature dependence of solar cell parameters. *Solar Cells* 17(2), 309–315. [https://doi.org/10.1016/0379-6787\(86\)90020-7](https://doi.org/10.1016/0379-6787(86)90020-7)
- Fathi, M., Abderrezek, M., Djahli, F., Ayad, M. (2015) Study of Thin Film Solar Cells in High Temperature Condition. *Energy Procedia* 74, 1410–1417. <https://doi.org/10.1016/j.egypro.2015.07.788>
- Frisk, C., Platzer-Björkman, C., Olsson, J., Szaniawski, P., Wätjen, J.T., Fjällström, V., Salomé, P., Edoff, M. (2014) Optimizing Ga-profiles for highly efficient $\text{Cu}(\text{In,Ga})\text{Se}_2$ thin film solar cells in simple and complex defect models. *J. Phys. D: Appl. Phys.*, 47, 485104. <https://doi.org/10.1088/0022-3727/47/48/485104>
- Ghani, F., Duke, M., Carson, J. (2013) Numerical calculation of series and shunt resistance of a photovoltaic cell using the Lambert W-function: Experimental evaluation. *Solar Energy* 87, 246–253. <https://doi.org/10.1016/j.solener.2012.11.002>
- Goffard, J., Colin, C., Mollica, F., Cattoni, A., Sauvan, C., Lalanne, P., Guillemoles, J.-F., Naghavi, N., Collin, S. (2017) Light Trapping in Ultrathin CIGS Solar Cells with Nanostructured Back Mirrors. *IEEE J. Photovoltaics* 7, 1433–1441. <https://doi.org/10.1109/JPHOTOV.2017.2726566>
- Gremenok, V.F., Zaretskaya, E.P., Bashkirov, S.A., Kim, W.Y., Chai, S.H., Moon, C.-B., Jhun, C.G. (2015) Growth and Optical Properties of $\text{Cu}(\text{In,Ga})\text{Se}_2$ Thin Films on Flexible Metallic Foils. *J. Adv. Microsc. Res.*, 10, 28–32; <https://doi.org/10.1166/jamr.2015.1233>
- Igalson, M., & Urbaniak, A. (2005) Defect states in the CIGS solar cells by photocapacitance and deep level optical spectroscopy. *Bulletin of the Polish Academy of Sciences: Technical Sciences*, 53 (2), 157-161.
- Kerr, L.L., Li, S.S., Johnston, S.W., Anderson, T.J., Crisalle, O.D., Kim, W.K., Abushama, J., Noufi, R.N. (2004) Investigation of defect properties in $\text{Cu}(\text{In,Ga})\text{Se}_2$ solar cells by deep-level transient spectroscopy. *Solid-State Electronics* 48, 1579–1586. <https://doi.org/10.1016/j.sse.2004.03.005>
- Khan, S., Rashid, M., Rahim, W., Aitezaz Hussain, M., Rahim, A. (2020) Numerical Simulation for Enhancement of output Performance of WS_2 based Thin Film Solar Cells. *IJEW* 07, 149–153; <https://doi.org/10.34259/ijew.20.702149153>
- Kumar, A., Singh, S., 2020. Numerical modeling of planar lead free perovskite solar cell using tungsten disulfide (WS_2) as an electron transport layer and Cu_2O as a hole transport layer. *Mod. Phys. Lett. B* 34, 2050258; <https://doi.org/10.1142/S0217984920502589>
- Lin, Y., Adilbekova, B., Firdaus, Y., Yengel, E., Faber, H., Sajjad, M., Zheng, X., Yarali, E., Seitkhan, A., Bakr, O.M., El-Labban, A., Schwingenschlögl, U., Tung, V., McCulloch, I., Laquai, F., Anthopoulos, T.D. (2019) 17% Efficient Organic Solar Cells Based on Liquid Exfoliated WS_2 as a Replacement for PEDOT:PSS. *Adv. Mater.* 31, 1902965; <https://doi.org/10.1002/adma.201902965>
- Liu, S., Simburger, E., Matsumoto, J., Garcia, A., Ross, J., Nocerino, J. (2005) Evaluation of thin-film solar cell temperature coefficients for space applications. *Prog Photovolt Res Appl* 13, 149–156. <https://doi.org/10.1002/pip.602>
- Lundberg, O., Bodegård, M., Malmström, J., Stolt, L. (2003) Influence of the $\text{Cu}(\text{In,Ga})\text{Se}_2$ thickness and Ga grading on solar cell performance: CIGS thickness and Ga grading: solar cell performance. *Prog. Photovolt: Res. Appl.* 11, 77–88; <https://doi.org/10.1002/pip.462>
- Nakamura, M., Yamaguchi, K., Kimoto, Y., Yasaki, Y., Kato, T., Sugimoto, H. (2019) Cd-Free $\text{Cu}(\text{In,Ga})(\text{Se,S})_2$ Thin-Film Solar Cell With Record Efficiency of 23.35%. *IEEE J. Photovoltaics*, 9, 1863–1867; <https://doi.org/10.1109/JPHOTOV.2019.2937218>
- Ong, K.H., Agileswari, R., Maniscalco, B., Arnou, P., Kumar, C.C., Bowers, J.W., Marsadek, M.B. (2018) Review on Substrate and Molybdenum Back Contact in CIGS Thin Film Solar Cell. *International Journal of Photoenergy*, 1–14; <https://doi.org/10.1155/2018/9106269>
- Patel, A. K., & Pandey, B.P. (2020) Performance Analysis of WS_2 TMD Material as an absorber layer used in Solar Cell. (ICE3-2020)
- Pettersson, J., Torndahl, T., Platzer-Björkman, C., Hultqvist, A., Edoff, M., 2013. The Influence of Absorber Thickness on $\text{Cu}(\text{In,Ga})\text{Se}_2$ Solar Cells With Different Buffer Layers. *IEEE J. Photovoltaics*, 3, 1376–1382; <https://doi.org/10.1109/JPHOTOV.2013.2276030>
- Rai, N., & Dwivedi, D.K. (2020) Numerical modelling for enhancement of output performance of CIGS based thin film solar cell using SCAPS 1-D simulation software. ICC-2019, Bikaner, India, 140021; <https://doi.org/10.1063/5.0001233>
- Rashidi, S., Rashidi, S., Heydari, R.K., Esmaeili, S., Tran, N., Thangi, D., Wei, W. (2020) WS_2 and MoS_2 counter electrode materials for dye-sensitized solar cells. *Prog Photovolt Res Appl pip.3350*; <https://doi.org/10.1002/pip.3350>
- Ravindra, N.M., Lin, Liqi. (2020) Temperature dependence of CIGS and perovskite solar cell performance: an overview. *Applied Sciences* 2,1361. <https://doi.org/10.1007/s42452-020-3169-2>
- Roy, S., Bermel, P. (2018) Electronic and optical properties of ultra-thin 2D tungsten disulfide for photovoltaic applications. *Solar Energy Materials and Solar Cells*, 174, 370–379; <https://doi.org/10.1016/j.solmat.2017.09.011>
- Shanmugam, M., Bansal, T., Durcan, C.A., Yu, B. (2012) Schottky-barrier solar cell based on layered semiconductor tungsten disulfide nanofilm. *Appl. Phys. Lett.* 101, 263902; <https://doi.org/10.1063/1.4773525>
- Sharaman, W.N., Birkmire, R.W., Marsillac, S., Marudachalam, M., Orbey, N., Russell, T.W.F. (1997) Effect of reduced deposition temperature, time, and thickness on $\text{Cu}(\text{In,Ga})\text{Se}/\text{sub } 2/$ films and devices, in: Conference Record of the Twenty Sixth IEEE Photovoltaic Specialists Conference, 331–334; <https://doi.org/10.1109/PVSC.1997.654095>
- Singh, A.K., & Jen, T. C. (2020) Structural, optical properties of spin-coated CIG/SLG, CIGS/SLG, CIGS/Mo/SLG thin films. *Surface Engineering*, 36, 22–28; <https://doi.org/10.1080/02670844.2018.1535787>
- Sobayela, K., Shahinuzzaman, M., Amin, N., Karim, M.R., Dar, M.A., Gul, R., Alghoul, M.A., Sopian, K., Hasan, A.K.M., Akhtaruzzaman, Md. (2020) Efficiency enhancement of CIGS solar cell by WS_2 as window layer through numerical modelling tool. *Solar Energy* 207, 479–485; <https://doi.org/10.1016/j.solener.2020.07.007>
- Sobayelb, K., Rahman, K. S., Karim, M. R., Aijaz, M. O., Dar, M. A., Shar, M. A., Misran, H., Amin, N. (2018) Numerical Modeling on Prospective Buffer Layers for Tungsten Di-Sulfide (WS_2) Solar Cell by Scaps-1d, 15(6), 307-315.

Zaidi, B., Zouagri, M., Merad, S., Shekhar, C., Hadjoudja, B.,
Chouial, B. (2019) Boosting Electrical Performance of CIGS

Solar Cells: Buffer Layer Effect. Acta Phys. Pol. A 136, 988-
991. <https://doi.org/10.12693/APhysPolA.136.988>



© 2022. The Authors. This article is an open access article distributed under the terms and conditions of the Creative Commons Attribution-ShareAlike 4.0 (CC BY-SA) International License (<http://creativecommons.org/licenses/by-sa/4.0/>)